Honda Research Institute EU
Honda Research Institute Europe GmbH
https://www.honda-ri.de/

The effect of Reynolds number on a transonic swept fan OGV in a small turbofan engine

Toyotaka Sonoda, Toshiyuki Arima, Giles Endicott, Markus Olhofer, Bernhard Sendhoff

2012

Preprint:

This is an accepted article published in Proceedings of the ASME Turbo Expo. The final authenticated version is available online at: https://doi.org/[DOI not available]

Proceedings of ASME Turbo Expo 2012
GT2012
June 11-15, 2012, Copenhagen, Denmark

GT2012-69956

THE EFFECT OF REYNOLDS NUMBER ON A TRANSONIC SWEPT FAN OGV IN A SMALL TURBOFAN ENGINE

Toyotaka Sonoda
Honda R&D Co. Ltd.
Aircraft Engine R&D Center
1-4-1 Chuo, Wako-shi, Saitama 351-0193, Japan

Toshiyuki Arima
Honda R&D Co. Ltd.
Fundamental Technology Research Center
1-4-1 Chuo, Wako-shi, Saitama 351-0193, Japan

Giles Endicott
Honda Research Institute Europe GmbH
Carl-Legien-Str.30
D-63073 Offenbach/Main, Germany

Markus Olhofer
Honda Research Institute Europe GmbH
Carl-Legien-Str.30
D-63073 Offenbach/Main, Germany

Bernhard Sendhoff
Honda Research Institute Europe GmbH
Carl-Legien-Str.30
D-63073 Offenbach/Main, Germany

ABSTRACT

In this paper, Reynolds effects on a transonic swept fan outlet guide vane (OGV) in a small turbofan engine are evaluated using a CFD model, successfully assessed with respect to experimental data. The flow-fields are evaluated at two Reynolds number conditions, a high Reynolds condition (corresponding to take-off conditions) and a low Reynolds number condition (corresponding to cruise conditions). The CFD results show large differences in the overall OGV performance between these two points. The flow mechanism for the deterioration in the OGV's performance at the low Reynolds number condition is shown. Finally a new idea for improving the OGV performance is proposed.

INTRODUCTION

There are several publications on two dimensional compressor cascades at low Reynolds numbers. For example, Rhoden [1] reported that for very low speed cascades with a large camber angle a low pressure peak near the leading edge of the suction surface seems to be effective at preventing laminar separation. Furthermore, additional analysis is required to determine the important factors for boundary layer transition and laminar separation bubbles for very low Reynolds numbers (~40,000 to ~250,000) (e.g. [2]). Authors previously reported that in the low Reynolds number regime airfoils with extreme front loading are superior to conventional controlled diffusion airfoils (CDA) which have a suction side velocity maximum around 20% of chord [3-5]. In case of the extremely front loaded airfoil, rapid deceleration causes early boundary layer transition and helps to avoid extended and unstable laminar separation bubbles which induce additional total pressure losses.

On the other hand, there are few papers on the effect of Reynolds number on three dimensional compressor blades, especially for a transonic fan OGV in turbofan engines. This is because the OGVs that have been investigated are predominantly used for medium or large sized turbofan engines, and therefore there have been no significant issues due to Reynolds effect. When applied to smaller sized turbofan engines, the OGV performance appears to be affected by Reynolds effects and therefore it is worth investigating the Reynolds effects when looking for more compact transonic OGV design solutions. The OGV used in this paper is an optimized transonic swept fan OGV with a novel wave type casing profile resulting from numerical optimization techniques and the optimized OGV reduces the loss by about 20% dramatically over a wide operating range from near choke to near stall [6]. The aerodynamic design concept has been shown in [7], in more detail.

The main objective in this paper is to investigate the effect of Reynolds number on the transonic swept fan OGV performance in a small turbofan engine.

Copyright © 2012 by ASME

NOMENCLATURE

M	Mach number
Re	Reynolds number based on mid-span chord length
RT	distance in circumferential direction
r	distance in radial direction
X	distance in axial direction

Subscripts

2	outlet station of rotor / inlet station of OGV
3	outlet station of downstream of OGV
ax	axial
is	isentropic process value

Abbreviations

CFD	computational fluid dynamics
EXP	experiment
LE	leading edge
NC	near choke
NS	near stall
OGV	outlet guide vane
PE	peak efficiency
SS	suction side,

APPROACH

Optimized OGV

The passage geometry for the optimized blade discussed is shown in Fig. 1 [6]. In comparison to the baseline, the passage has been significantly moved radially outward, together with modifications to the passage profile. The optimal design incorporates an unconventional oscillatory profile with the maximum passage area at around 20% of the OGV chord, before a significant contraction, with minimal area close to the trailing edge. The detailed definition of the first and second concave surfaces is described in [7].

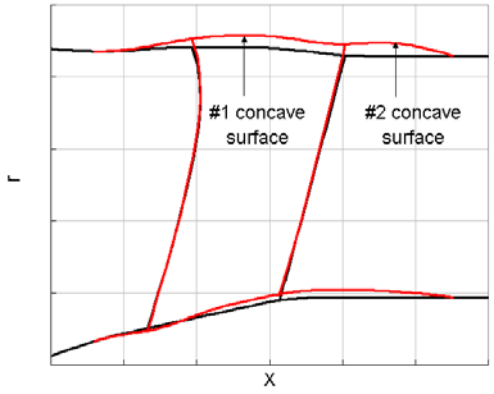

Fig. 1 Comparison of meridional passage geometry, baseline OGV: "black", optimized OGV: "red".

Flow Solver

For the simulation of the fluid dynamic properties of the blade designs the parallelized 3D in-house Reynolds-averaged Navier-Stokes (RANS) flow solver HSTAR (Honda Software for Turbomachinery Aerodynamics Research) [8] was used. For turbulence modeling, Menter's k-ω SST turbulence model [9] was chosen because it gave the best agreement between CFD and experimental data for the baseline blade geometry.

As pointed out by Rumsey and Spalart [10], the k-omega SST model has a well-defined transition location for levels of free-stream turbulent intensity (Tu) and eddy viscosity ratio (μ_T/μ), however it is incapable of predicting re-laminarization. The boundary conditions for the turbulence model are modeled based on inlet turbulence levels, namely, Tu=5% and μ_T/μ=100. Such a high level of free stream turbulence activates the model immediately at the blade leading edge and on the casing walls. Due to this, a numerical investigation is carried out of the effect of Reynolds number that corresponds to the turbulent boundary layer development.

In order to sufficiently resolve the boundary layer development, CFD simulations were performed in advance to determine the number of cells required to obtain grid independence. The chosen computational grid consisted of 201 nodes in the stream-wise direction, 81 nodes in the radial direction, and 61 nodes in the circumferential direction (totaling approximately one million cells).

The computational OGV grid for the baseline blade used in the simultaneous optimization of both airfoil and axisymmetric end-wall contouring outlined in [6] is shown in Fig. 2-top. The grid is composed of three parts: tip end-wall part, hub end-wall part, and the actual airfoil. The airfoil tip and hub part grids were extended from the tip and hub end-walls so that the passage contours could be optimized. Flow direction is from "left" to "right" and the position of station 2 and 3 are the inlet and outlet stations of the swept OGV, respectively. Also the detail grid at the airfoil frontal part is shown in Fig. 2-bottom.

Essentially, the same grid was used for both the high Re and low Re CFD simulations. Firstly the grid for the high Reynolds number condition, that is, for the Full scale OGV configuration has been constructed to have y+ close to 1.0 for all calculations. After that, the grid is automatically scaled down to be the target of low Reynolds number condition. Therefore the y+ for the low Reynolds number condition should be smaller, due to the thicker inlet boundary layer.

The reason why the geometry scale factor was used instead of the cruise case atmosphere boundary condition is, as follows. In this research, a small scale fan stage rig with a ground atmospheric inlet condition that corresponds to the cruise (low Reynolds number) condition is usually used to assess stage performance experimentally. This is convenient as it reduces both development time and costs. The CFD code used has been carefully assessed by the experimental data obtained from the low Reynolds number condition. Therefore

Copyright © 2012 by ASME

in the case of the high Reynolds number condition the blade geometry is scaled up to be the target value.

For the inlet boundary condition, the span-wise distribution of total pressure, total temperature and flow angle, obtained from the small scale rig testing, are set. The inlet boundary layer thickness is "zero" at the starting grid point. The normalized overall span-wise total pressure distribution and the boundary layer thickness just upstream of the LE for two Reynolds number conditions (red: high Re, blue: low Re) are shown in Fig. 3-left and right, respectively, in the form of the normalized span-wise total pressure distribution. In the right figure, the hub region (0% to 5% span-height) in the left figure is enlarged. It can be seen that the boundary layer thickness for the low Reynolds number case is about twice that of the high Reynolds number case.

The computation for one flow analysis with this grid takes roughly 50 minutes on an Intel Xeon5570 2.93 GHz Quad-Core processor using the Intel MPI library.

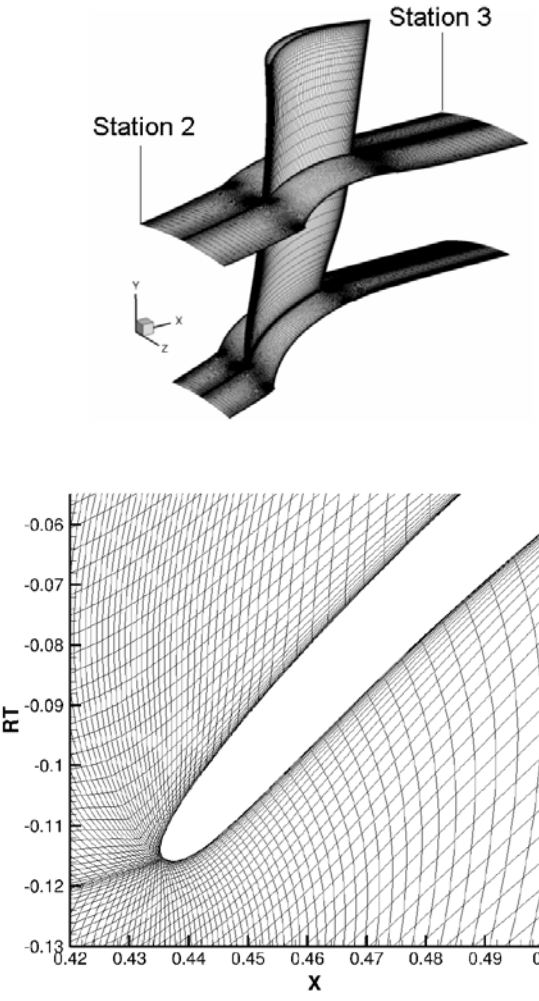

Fig. 2 Structured computational mesh, top: overall view, bottom: frontal part of baseline OGV at 5% span-height.

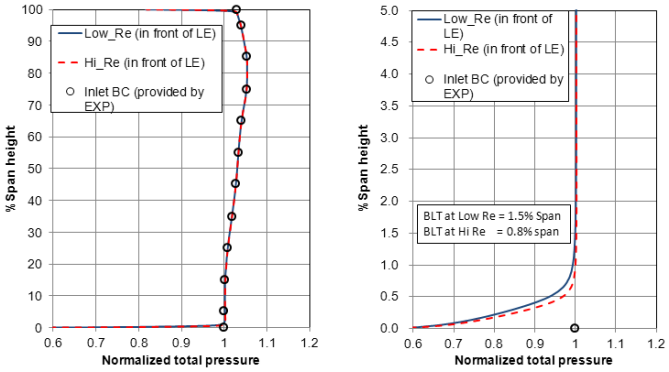

Fig. 3 Comparison of inlet boundary layer thickness at just upstream of OGV LE.

Assessment of Flow Solver

The comparison between physical experimentation and simulations (CFD) of both the circumferential and span-wise averaged total pressure loss for the baseline OGV is shown in Fig. 4. The vertical axis of the OGV total pressure loss and the horizontal axis of the mass flow rate are normalized by experimental value of the baseline overall OGV total pressure loss and the mass flow rate at the design point (P2, here we call this "PE-point") for cruise operating condition. It can be seen that there is a sudden increase of loss near the choke side, whereas a gradual increase of the loss can be observed near the stall side. In general, there is a very good qualitative and quantitative agreement between experimental and computation results.

Further details on the assessment of the CFD solver, for example, span-wise OGV total pressure loss distribution at design and off-design points, is shown in [7]. In the CFD, Reynolds numbers for cruise and take-off conditions are adjusted by changing the OGV geometry-scale factor itself.

RESULTS AND DISCUSSION

According to the CFD assessment discussed previously, there is good agreement for the overall loss value simulation (see Fig. 4), despite the fact that in this computational simulation a transition model is not used.

Reynolds Effect on Overall Performance

Figure 5 shows the effect of Reynolds number on the optimized OGV loss and mass flow rate at high Re (take-off) and low Re (cruise) conditions. The vertical axis (loss) is once again normalized by the experimental value of the baseline design's overall OGV total pressure loss at the design point (PE-point) for the cruise condition. The OGV loss is significantly increased for the entire mass flow rate range as the Reynolds number is decreased. The impact of the loss variation from the high Re number (take-off) to the low Re number is not small. It corresponds to over a 0.5% drop in

Copyright © 2012 by ASME

stage efficiency. Therefore it is important to clarify the flow mechanism for the loss increase at the low Reynolds number. Also, it can be seen that the mass flow rate is significantly reduced by about 1.4% at NC and about 1.8% at NS, as the Reynolds number is decreased. A steep increase of the loss is observed at NC in the low Reynolds number condition.

Figure 6 shows the circumferentially averaged span-wise total pressure loss coefficient for the optimized OGV at take-off (high Re) and cruise (low Re) conditions. The significant increase of the loss is observed at around 10% and around 85% span-heights. It seems that there is an influence of corner stall and/or secondary flow, developed on both hub and tip casings.

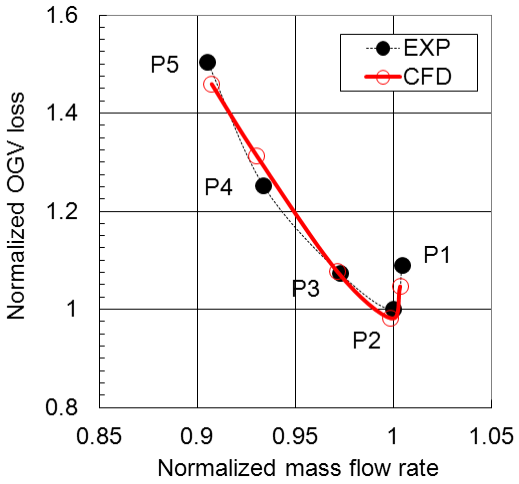

Fig. 4 Assessment of CFD code on normalized overall OGV loss for baseline OGV under low Reynolds number (cruise) condition.

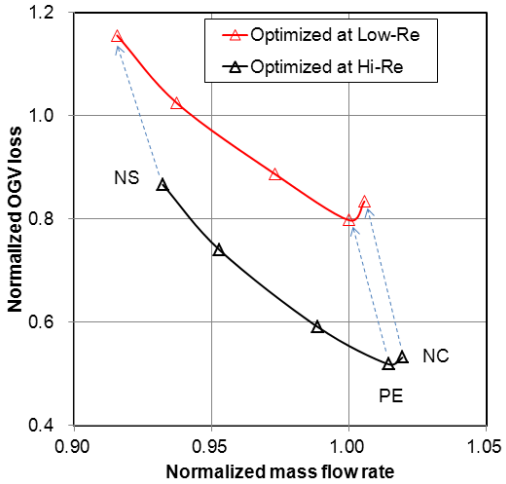

Fig. 5 The Effect of Reynolds number on the optimized OGV loss and mass flow rate, red: low Re, black: high Re.

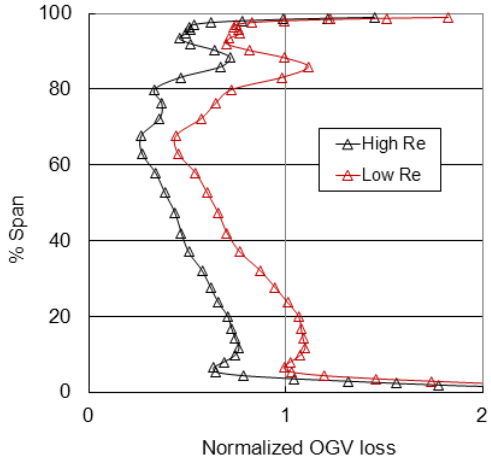

Fig. 6 Span-wise total pressure loss distribution at low and high Reynolds numbers for optimized OGV.

The upper half of Figure 7 shows the blade surface isentropic Mach number distribution for the optimized OGV at high and low Reynolds numbers. At both Reynolds numbers, a more frontally loaded blade surface Mach number distribution is obtained, when compared to the baseline OGV (see Fig. 7-bottom). In the case of the low Reynolds number, the blade loading around the frontal part of the airfoil with the high curvature region is significantly reduced, probably due to the reduced mass flow rate (see Fig.5). It is also interesting to note that an irregular pattern of Mach number distribution, observed around the leading edge at 5% span in the high Reynolds number condition for the baseline OGV, has disappeared at low Reynolds number condition.

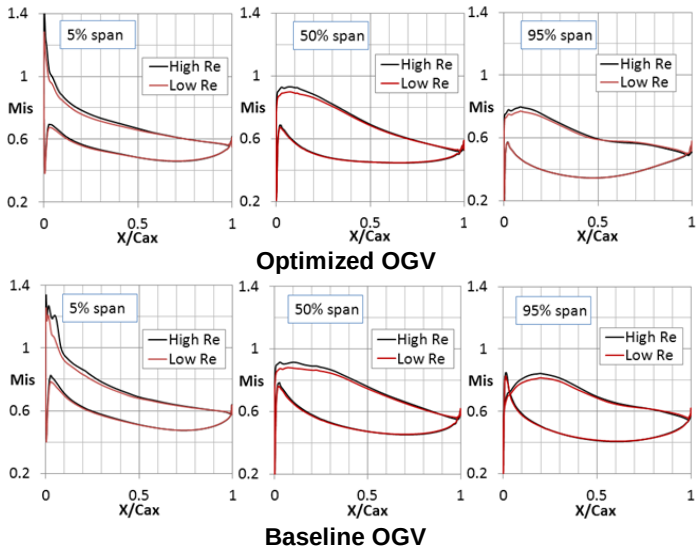

Fig. 7 Blade surface isentropic Mach number distribution for optimized OGV (top) and baseline OGV (bottom) at three span heights, left: 5% span, middle: 50% span, and right: 95% span, at PE point.

Copyright © 2012 by ASME

In order to investigate the reason why the irregular pattern exists, additional analysis was performed. Figure 8-top shows blade to blade Mach number contours around the LE at 5% span-height for the baseline blade. The left side is for the high-Reynolds number and the right side is for the low Reynolds number. In the case of high Reynolds number the concentrated Mach number lines normal to the airfoil surface point A are observed, like a normal shock. Also there seems to be a weak shock around between points B and C, where the Mach number is slightly decreased and also the pattern is slightly deformed. On the other hand, in the case of the low Reynolds number there is no such tendencies observed in the case of the high Reynolds number.

In order to confirm the previous discussion, Schlieren pictures which visualize the density gradients were used. Schlieren photos not only make shocks, wakes and separation zones visible but also allow the recognition of regions of flow deceleration and acceleration. As shown in Fig. 8-middle, the shock pattern around point A is very clear, although the shock pattern between points B and C is not clear. On the other hand in the case of the low Reynolds number (see middle-right figure), there is no clear shock. Therefore it can be said that there are Reynolds effects on the shock pattern, although the inlet Mach number is slightly decreased about 1.4% (see Fig. 5). Additionally it is very clear the boundary layer separation on SS in the case of the low Reynolds number is larger than that in the case of the high Reynolds number, as shown in Fig. 8-bottom.

Flow Mechanism

Figure 9 shows the numerical oil flow pattern for the optimized OGV at high (take-off) and low (cruise) Reynolds numbers. At the high Reynolds number condition, corner stalls around both hub and tip are observed and there is no boundary layer separation in the remaining mid-span region. At the low Reynolds number, there is no separation around the frontal part of the airfoil in the mid-span, but both corner stalls have developed further separation. Therefore the main reason why the OGV loss increases when Reynolds number decreases is due to the larger corner stalls in the hub and tip regions.

The reason the corner stall increases with decreasing Reynolds number is mainly due to stronger viscous effects (a thicker inlet boundary layer) on the end-wall, as shown in Fig. 10 and 11. That is: Figure 10 shows the comparison of hub end-wall static pressure contours and oil flow traces at high (left) and low (right) Reynolds numbers. The most notable feature is the position of a horseshoe vortex is shifted upstream due to the thicker inlet boundary layer at the low Reynolds number condition. As a result, a larger low-momentum fluid migration occurs in a blade to blade sense on the hub end-wall and this results in a larger span-wise migration toward the mid-span along the suction surface (see Fig. 9). In the case of the tip end-wall (see Fig. 11) the flow characteristics are very similar to the hub end-wall pattern (see Fig. 10).

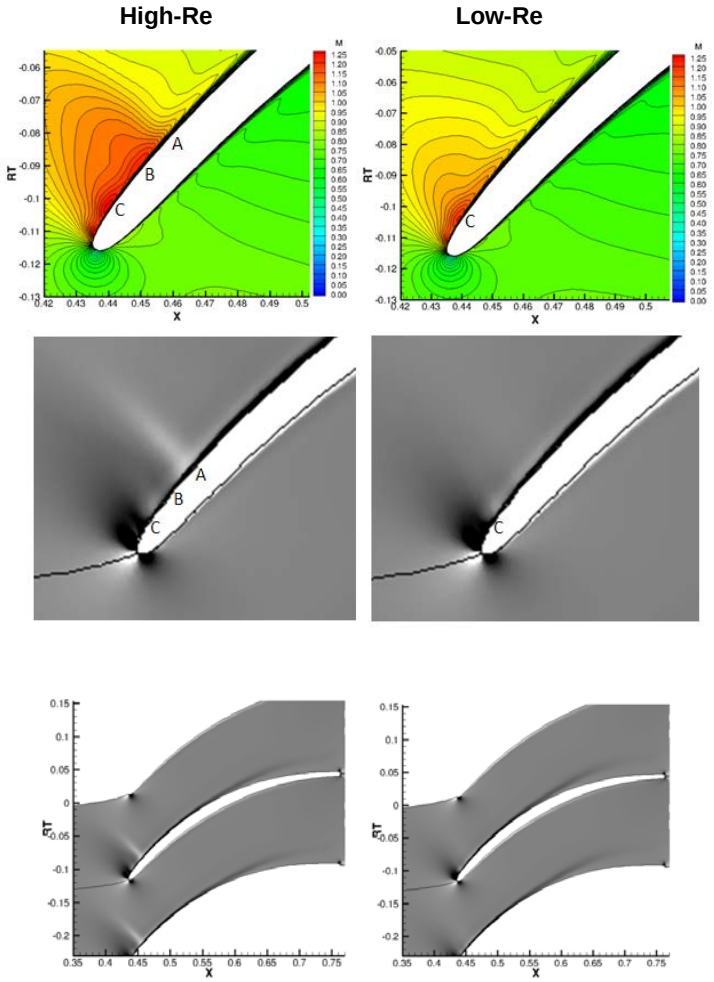

Fig. 8 Effect of Reynolds number on Mach number contours (top) and shock pattern (middle and bottom) at 5% span-height for baseline OGV.

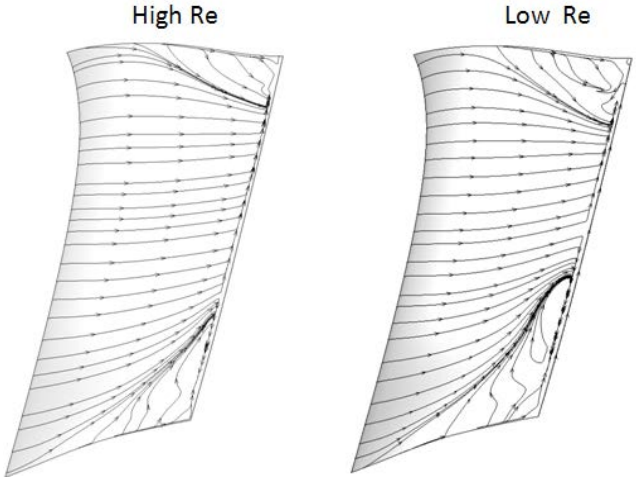

Fig. 9 Comparison of numerical oil flow pattern on optimized OGV suction surface, left: high Re, right: low Re.

Copyright © 2012 by ASME

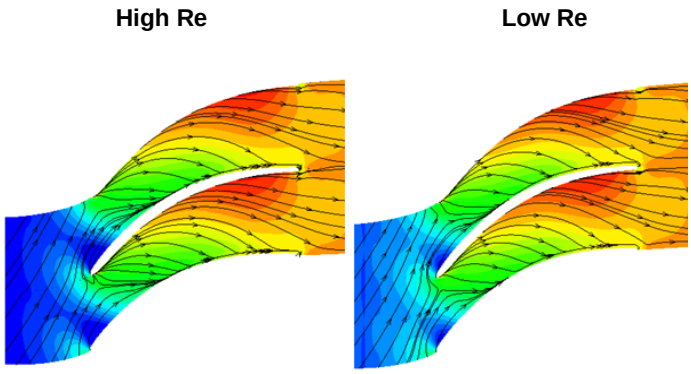

Fig. 10 Comparison of hub end-wall static pressure contours at PE point for optimized OGV, left: high Re, right: low Re.

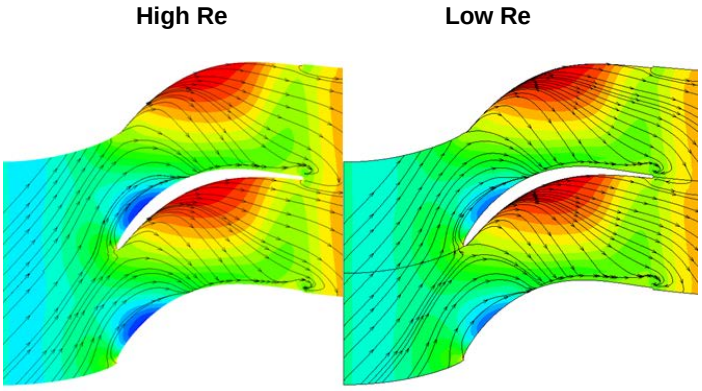

Fig. 11 Comparison of tip wall static pressure contours at PE point for optimized OGV, left: high Re, right: low Re.

So far, the flow mechanism describing why the OGV loss is increased when the Reynolds number is decreased has been discussed. In order to confirm this, a particle trace method was performed.

Figure 12 shows the comparison of particle traces released at the same spatial positions upstream of the optimized OGV LE (blade suction surface and static pressure contours are also shown and the axial flow direction is from right to left). In the case of the low Reynolds number condition, the hub corner stall is enhanced within the passage, and after that, the downstream particle traces in the wake are more dispersed toward the mid-span, when compared to the high Reynolds number condition. This is the primary reason why losses between around 10% span-height and around 70% span-height are increased, as shown in Fig. 6.

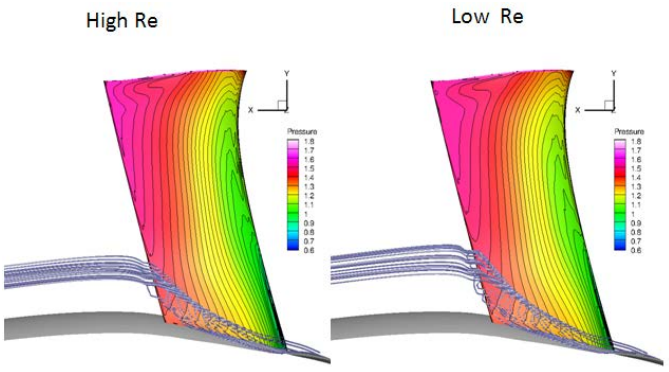

Fig. 12 Comparison of particle traces and static pressure contours for the optimized OGV at PE point, left: high Re, right: low Re.

How to reduce Reynolds effect

As already shown in Fig. 5, there are clearly Reynolds effects on the transonic swept fan OGV loss. The primary reason for the larger corner stall observed on the swept OGV at low Reynolds number seems to be the result of a combination of a “thicker inlet boundary layer” combined with a “slanted iso-static pressure line”, a unique characteristic of a swept OGV, shown in Fig. 13. That is, in the case of a swept blade the iso-static pressure lines are observed to be more slanted to the horizontal, when compared to an un-swept (straight) blade. This means the migration of low-momentum fluid toward the mid-span is accelerated by the swept airfoil, because there is a negative pressure gradient along the span in an ideal case.

Therefore asymmetric end-wall contouring, focusing on both suppressing the low momentum fluid migration on the end-wall and creating less slanted (more vertical) iso-static pressure lines on the swept OGV suction surface seems to be needed.

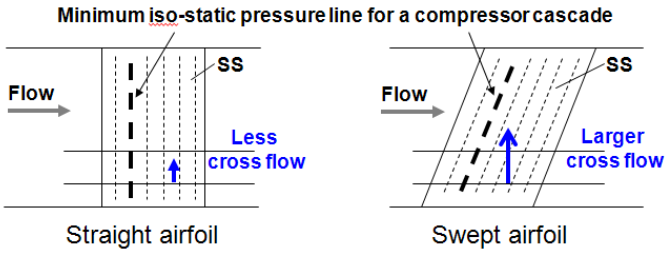

Fig. 13 Schematic figures of relation between suction surface iso-static pressure lines and low-momentum fluid migration.

Copyright © 2012 by ASME

CONCLUSIONS

In this paper, Reynolds effects and the aerodynamic characteristics of a transonic swept outlet guide vane (OGV) with a unique wave type casing profile in a small turbofan engine have been investigated to clarify whether Reynolds effects exist between take-off and cruise conditions. For the analysis we used 3D CFD simulations, assessed using experimental data from the baseline OGV blade. The following conclusions can be drawn.

- There are clearly Reynolds effects where the OGV loss is dramatically increased as Reynolds number is decreased from take-off to cruise conditions.

- The main reason why the OGV loss increases with decreasing Reynolds number is the larger corner stalls in the hub and tip regions.

- The flow mechanism causing this performance deterioration around both the hub and tip end-wall regions in the low Reynolds number condition is due to a combination of a thicker inlet boundary layer with slanted iso-static pressure lines on the OGV suction surface, a unique characteristic of the swept OGV.

- A further study seems to be needed, focusing on both suppressing low momentum fluid migration on the end-wall and creating a less slanted iso-static pressure line on the swept OGV suction surface, by using asymmetric end-wall contouring.

REFERENCES

[1] Rhoden, H.G., 1952, “Effects of Reynolds Number on the Flow of Air through a Cascade of Compressor Blades,” ARC, R&M No. 2919.

[2] Roberts, W.B., 1975, “The Effect of Reynolds Number and Laminar Separation on Axial Cascade Performance,” ASME *Journal of Engineering for Power*, Vol. 97, pp. 261-274.

[3] Sonoda, T., Yamaguti, Y., Arima, T., Olhofer, M., Sendhoff, B., Schreiber, H. A., 2004, “Advanced High Turning Compressor Airfoils for Low Reynolds Number Condition, Part 1: Design and Optimization”, ASME *Journal of Turbomachinery*, Vol. 126, No. 3, pp.350-359.

[4] Schreiber, H.A., Steinert, W., Sonoda, T., and Arima, T., 2004, “Advanced High Turning Compressor Airfoils for Low Reynolds Number Condition, Part 2: Experimental and Numerical Analysis,” ASME *Journal of Turbomachinery*, Vol. 126, No. 4, pp. 482-492.

[5] Sonoda, T., and Schreiber, H.A., 2007 “Aerodynamic Characteristics of Supercritical Outlet Guide Vanes at Low Reynolds Number Conditions”, ASME *Journal of Turbomachinery*, Vol. 129, No. 4, pp. 694-704.

[6] Endicott, G., Sonoda, T., Olhofer, M., and Arima, T., 2011, “Aerodynamic Improvement of A Transonic Fan Outlet Guide Vane Using 3D Design Optimization,” 2011, ASME Paper GT2011-46363.

[7] Sonoda, T., Arima, T., Endicott, G., Olhofer, M., 2011, “A New Aerodynamic Design Concept for Transonic Swept Fan Outlet Guide Vanes,” ISABE-2011-1224.

[8] Arima, T., Sonoda, T., Shirotori, M., Tamura, A., and Kikuchi, K., 1999, “A Numerical Investigation of Transonic Axial Compressor Rotor Flow Using a Low-Reynolds-Number k-ε Turbulence Model,” ASME *Journal of Turbomachinery*, Vol. 121, pp.44-58.

[9] Menter, F. R., 1994, "Two-Equation Eddy-Viscosity Turbulence Models for Engineering Applications," AIAA Journal, Vol. 32, No. 8, pp. 1598-1605.

[10] Rumsey, C. L. and Spalart, P. R., 2008, “Turbulence Model Behavior in Low Reynolds Numbers Regions of Aerodynamic Flow Fields,” IAAA-Paper 2008-4403.

Copyright © 2012 by ASME